

# Enhanced Estimation Techniques for Certified Radii in Randomized Smoothing

Zixuan Liang

zliang1@my.harrisburgu.edu

**Abstract**—This paper presents novel methods for estimating certified radii in randomized smoothing, a technique crucial for certifying the robustness of neural networks against adversarial perturbations. Our proposed techniques significantly improve the accuracy of certified test-set accuracy by providing tighter bounds on the certified radii. We introduce advanced algorithms for both discrete and continuous domains, demonstrating their effectiveness on CIFAR-10 and ImageNet datasets. The new methods show considerable improvements over existing approaches, particularly in reducing discrepancies in certified radii estimates. We also explore the impact of various hyperparameters, including sample size, standard deviation, and temperature, on the performance of these methods. Our findings highlight the potential for more efficient certification processes and pave the way for future research on tighter confidence sequences and improved theoretical frameworks. The study concludes with a discussion of potential future directions, including enhanced estimation techniques for discrete domains and further theoretical advancements to bridge the gap between empirical and theoretical performance in randomized smoothing.

**Index Terms**—certified radii, randomized smoothing, neural network robustness, adversarial machine learning, probabilistic certification, robustness radius, hyperparameter tuning

## I. Introduction

Deep neural networks (DNNs) have transformed fields such as computer vision [1] and natural language processing [2], excelling in tasks by learning complex patterns [3]. Their integration into critical systems, including smartphones and autonomous vehicles, has highlighted significant security concerns [4], [5]. Addressing these vulnerabilities is crucial, particularly in adversarial machine learning, which focuses on defending against malicious attacks [6].

Adversarial examples, subtly perturbed inputs that mislead DNNs [7], [8], pose threats across domains like image classification [9], speech recognition [10], and autonomous systems [11], [12]. In healthcare, adversarial manipulations can cause misdiagnoses [13], while in finance, they could undermine fraud detection and trading algorithms [14], [15].

Defense strategies include adversarial training [16], input preprocessing [17], and detection [18]. Despite progress, these methods face challenges like increased computational costs and limited generalization [19], [20]. Certifiable robustness approaches offer formal guarantees, leveraging methods such as MILP [21], SMT [22], and randomized smoothing [23]. While scalable, these techniques often yield conservative bounds [24], [25].

Emerging probabilistic certifications like randomized smoothing balance scalability and rigor, making them promising for state-of-the-art architectures [23]. As DNNs become ubiquitous, securing them requires a multifaceted approach, blending empirical defenses, formal verification, and innovative designs. The following sections explore randomized smoothing in detail, emphasizing its theoretical underpinnings and practical applications.

In summary, this paper is structured as follows:

- Section II introduces the theoretical foundations of randomized smoothing, along with the notations and definitions used throughout.
- Section III precisely formulates the problem, dividing it into two subproblems: the discrete case and the continuous case.
- Section IV addresses the discrete case, presenting our initial contributions.
- Section V begins with a novel formulation of confidence intervals in Subsection V-A and extends the discussion to contributions for the continuous case.
- Section VI validates the theoretical results on real-world datasets, including CIFAR-10 and ImageNet.

## II. Background & Related Work

### A. Notation

Following [26], let  $\mathcal{X} \subset \mathbb{R}^d$  denote the input space and  $\mathcal{Y} = \{1, \dots, m\}$  represent the set of  $m$  class labels. For a data point  $x \in \mathcal{X}$  with true label  $y \in \mathcal{Y}$ , a neural network classifier  $F_{out} : \mathcal{X} \rightarrow \mathcal{Y}$  predicts as:

$$F_{out}(x) = \arg \max_{k \in \mathcal{Y}} s_k \circ f(x),$$

where  $f : \mathcal{X} \rightarrow \mathbb{R}^m$  outputs logits and  $s : \mathbb{R}^m \rightarrow \Delta^{m-1}$  is the normalizing layer projecting onto the  $(m-1)$ -dimensional probability simplex:

$$\Delta^{m-1} := \left\{ p \in \mathbb{R}^m : p_i \geq 0, \sum_{i=1}^m p_i = 1 \right\}.$$

The composed classifier  $F := s \circ f$  outputs a probability distribution over  $m$  classes, termed the **soft classifier**, while  $F_{out}$  is the **hard classifier**. Common simplex maps include softmax [27], hardmax (assigning all mass to the maximum component), and sparsemax [28], which is the Hilbert projection onto the simplex. We refer to the hardmax-based case as the **discrete case** and cases using continuous projections (e.g., softmax or sparsemax) as the **continuous case**.

## B. Randomized Smoothing

Randomized smoothing enhances classifier robustness against small adversarial perturbations by stabilizing decisions under random input noise. This concept, formalized via the robustness radius in Section II-C, intuitively implies that stable predictions under perturbation yield higher robustness.

Figure 1 from [23] illustrates this process. The left image depicts a clean input  $x$  (a panda image), while the right image shows its perturbed version, generated by applying Gaussian noise with  $\sigma = 0.5$ . The smoothed classifier aggregates predictions over such noisy samples to improve robustness.



Fig. 1. Randomized smoothing: Left, original image  $x$  (panda). Right, image with Gaussian noise ( $\sigma = 0.5$ ). The smoothed classifier predicts based on majority voting over noisy samples, mitigating smaller adversarial attacks.

Randomized smoothing enhances robustness by stabilizing predictions under random Gaussian perturbations. The smoothed classifier  $\hat{F} : \mathcal{X} \rightarrow \Delta^{m-1}$  implements a majority vote over soft classifier predictions under noise:

$$\hat{F}(x) := \mathbb{E}_{\epsilon \sim \mathcal{N}(0, \sigma^2 I)} [F(x + \epsilon)],$$

where  $\epsilon \sim \mathcal{N}(0, \sigma^2 I)$  represents isotropic Gaussian noise. The final classifier is:

$$\hat{F}_{out}(x) = \arg \max_{k \in \mathcal{Y}} \hat{F}_k(x).$$

This expectation is equivalent to convolving  $F$  with the Gaussian kernel  $p_\sigma$ , where:

$$p_\sigma(z) := \frac{1}{(2\pi\sigma^2)^{d/2}} \exp\left(-\frac{\|z\|^2}{2\sigma^2}\right).$$

## C. Robustness Radius

The certified radius  $R(F, x)$  quantifies robustness, representing the maximum perturbation  $\epsilon$  that keeps the classifier output consistent. Larger  $R(F, x)$  implies greater robustness.

For randomized smoothing with  $\ell_2$ -norm, the certified radius is:

$$R(F, x) = \begin{cases} 0, \\ \min \{ \epsilon > 0 \mid \exists \tau \in B_2(0, \epsilon), F_{out}(x + \tau) \neq y \}, \end{cases}$$

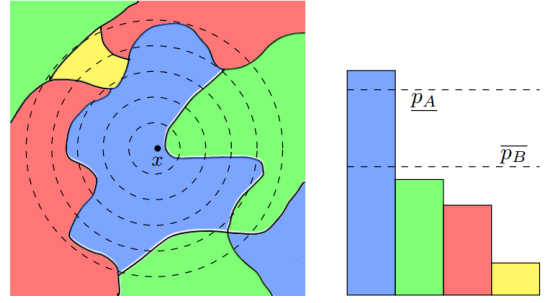


Fig. 2. Robustness radius: Left, decision boundaries with perturbation radii around  $x$ . Right, class probabilities vs. radius.  $\underline{p}_A$  and  $\overline{p}_B$  denote bounds for top-two class probabilities.

## D. Certified Radius and Lipschitz Constant

Lipschitz continuity relates to robustness: for a Lipschitz constant  $L$ ,

$$\|F(x_1) - F(x_2)\| \leq L \cdot \|x_1 - x_2\|.$$

The prediction margin  $M(F, x)$  quantifies confidence:

$$M(F, x) := F(x)_y - \max_{i \neq y} \{F(x)_i\}.$$

The certified radius is bounded as:

$$R(F, x) \geq \frac{M(F, x)}{\sqrt{2}L(F)}.$$

For a smoothed classifier  $\hat{F}$ , Lipschitz continuity provides:

$$R_1(\hat{F}, x) := \frac{M(\hat{F}, x)}{\sqrt{2}L(f)}.$$

## E. Certified Radius and Noise Magnitude

Cohen et al. define a second radius for randomized smoothing:

$$R_2(\hat{F}, x) = \frac{\sigma}{2} \left( \Phi^{-1}(\hat{F}(x)_y) - \Phi^{-1}(\max_{i \neq y} \{\hat{F}(x)_i\}) \right),$$

where  $\Phi$  is the Gaussian CDF. Larger  $\sigma$  increases robustness but may reduce accuracy on clean inputs, presenting a trade-off.

## III. Problem Formulation

### A. Monte Carlo Simulation

Certified radii (??) and (??) depend on evaluating the smoothed classifier  $\hat{F}$ , which involves intractable integrals. Monte Carlo methods approximate this by generating Gaussian noise samples, perturbing  $x$ , and evaluating the base classifier  $F$ . This approximation is scalable to high-dimensional data and large networks. Using the law of large numbers, the empirical distribution of outputs converges to the true smoothed classifier's distribution as the number of samples  $n$  increases.

#### 1) Discrete Case

if  $F_{out}(x) \neq y$ ,  
For discrete classifiers,  $F$  outputs one-hot vectors (class labels).  
A vector of counts  $X = (X_1, \dots, X_m)$  is generated by

sampling  $n$  noise instances  $\epsilon_i \sim \mathcal{N}(0, \sigma^2 I)$ , perturbing  $x$ , and evaluating  $F$ . Algorithm 1 outlines this.  $X$  approximates a multinomial distribution with  $n$  trials and probabilities  $p = (p_1, \dots, p_m)$ , where  $p_k = \mathbb{P}(f(x + \epsilon) = k)$ . The final prediction is  $\hat{F}_{out}(x) = \arg \max_k X_k$ . Confidence intervals for  $p_k$  (e.g., Clopper-Pearson) ensure robustness by bounding class probabilities.

---

### Algorithm 1: Sampling in the Discrete Case

---

**Input:** Base classifier  $F$ , number of samples  $n$ , standard deviation  $\sigma$ , and input  $x$

**Output:** Vector of counts  $X = (X_1, \dots, X_m)$

```

1 Initialize  $X = (0, \dots, 0)$ 
2 for  $i = 1$  to  $n$  do
3   Generate noise  $\epsilon_i \sim \mathcal{N}(0, \sigma^2 I)$ 
4    $\tilde{x}_i = x + \epsilon_i$ 
5    $y_i = F(\tilde{x}_i)$ 
6   Increment  $X_{y_i}$  by 1
7 end
8 return  $X$ 

```

---

## 2) Continuous Case

For continuous classifiers  $F : \mathbb{R}^d \rightarrow \Delta^{m-1}$ , a matrix  $X \in \mathbb{R}^{n \times m}$  is generated, where each row represents the classifier's output for a noisy sample. Algorithm 2 outlines the process.

The mean confidence for class  $k$  is computed as:

$$\hat{p}_k = \frac{1}{n} \sum_{i=1}^n X_i^k$$

This approximates the smoothed classifier's probabilities. The predicted output of the smoothed classifier is:

$$\hat{F}_{out}(x) = \arg \max_k \hat{p}_k$$

Confidence intervals are incorporated to account for variability in class probabilities, ensuring robust statistical estimates.

---

### Algorithm 2: Sampling in the Continuous Case

---

**Input:** Base classifier  $F : \mathbb{R}^d \rightarrow \Delta^{m-1}$ , number of samples  $n$ , standard deviation  $\sigma$ , and input  $x$

**Output:** Matrix  $X \in \mathbb{R}^{n \times m}$

```

1 Initialize  $X$  as an empty  $n \times m$  matrix
2 for  $i = 1$  to  $n$  do
3   Generate noise  $\epsilon_i \sim \mathcal{N}(0, \sigma^2 I)$ 
4    $\tilde{x}_i = x + \epsilon_i$ 
5    $y_i = F(\tilde{x}_i)$ 
6   Set the  $i$ -th row of  $X$  to  $y_i$ 
7 end
8 return  $X$ 

```

---

## B. Monte Carlo Approximation and Confidence Intervals

Monte Carlo introduces randomness into robustness certification, transforming the classifier into a stochastic model. Outputs are random vectors, enabling probabilistic analysis of variability and confidence. To avoid overestimation of robustness, one-sided lower bounds on the certified radius are used. This ensures

conservative guarantees even at the cost of slightly smaller radii.

Key trade-offs include: - **Sample Size ( $n$ ):** Larger  $n$  reduces confidence interval width, improving robustness estimates but increases computation. - **Confidence Level:** Higher levels (e.g., 99%) yield stronger guarantees but wider intervals and smaller radii.

Both discrete and continuous cases benefit from tighter bounds with increased  $n$ , but continuous classifiers offer statistical efficiency by retaining more information from  $F$ . Practical parameter choices (e.g.,  $n$ ,  $\sigma$ ) balance robustness, accuracy, and computational costs based on application requirements.

## C. Practical Calculation of Confidence Interval

To estimate certified radii, the core task involves calculating the prediction margin  $M(\hat{F}, x)$  or  $M(\Phi^{-1} \circ \hat{F}, x)$  using exact confidence intervals with Bonferroni correction, as outlined in Algorithm 3. Exact intervals guarantee robustness under high confidence, unlike approximate intervals which risk overestimation in extreme probabilities or small samples.

---

### Algorithm 3: Bonferroni approach for margin estimation

---

**Input:** Counts or grid matrix  $X$  and

getConfidenceBound() routine with confidence  $1 - \alpha$

**Output:** Margin  $M(\hat{F}, x)$  or  $M(\Phi^{-1} \circ \hat{F}, x)$  at confidence  $1 - \alpha$

```

1 Compute  $\hat{F}(x)_y$  for the true class using
  getConfidenceBound() at  $\frac{\alpha}{m}$ 
2 for all other classes  $j \neq y$  do
3   Compute  $\hat{F}(x)_j$  using getConfidenceBound()
  at  $\frac{\alpha}{m}$ 
4 end
5 Calculate  $M(\hat{F}, x)$  or  $M(\Phi^{-1} \circ \hat{F}, x)$ 
6 return  $M(\hat{F}, x)$  or  $M(\Phi^{-1} \circ \hat{F}, x)$ 

```

---

This conservative method ensures robustness guarantees by minimizing the confidence of the primary prediction while maximizing potential alternatives, providing a worst-case robustness scenario. In the discrete case, this focus is on the second-highest count due to the absence of variance within counts, ensuring a conservative robustness estimate.

Formally, for the second-highest class  $j$ :

$$M(\hat{F}, x) = \hat{F}(x)_y - \hat{F}(x)_j, \\ M(\Phi^{-1} \circ \hat{F}, x) = \Phi^{-1}(\hat{F}(x)_y) - \Phi^{-1}(\hat{F}(x)_j). \quad (1)$$

Using the Clopper-Pearson interval, let  $n_y$  and  $n_j$  represent the counts for the predicted and runner-up classes:

$$\underline{p}_y = \text{BetaInv}(\alpha/2, n_y, n - n_y + 1), \quad \bar{p}_j = \text{BetaInv}(1 - \alpha/2, n_j + 1, n - n_j) \\ \hat{M}(\hat{F}, x) = \underline{p}_y - \bar{p}_j, \quad \hat{M}(\Phi^{-1} \circ \hat{F}, x) = \Phi^{-1}(\underline{p}_y) - \Phi^{-1}(\bar{p}_j) \quad (2)$$

In the continuous case, confidence intervals are derived by inverting concentration inequalities. Variance-adaptive methods,

like Bernstein's inequality, yield tighter bounds in low-variance scenarios, whereas empirical Bernstein inequality estimates variance from samples, avoiding overly wide intervals seen with variance-agnostic methods like Hoeffding's.

These methods provide strong robustness guarantees by under-estimating the true margin, ensuring conservative robustness certificates even under probabilistic settings.

**Proposition 1** (Empirical Bernstein Inequality, [29]). *Let  $X_1, \dots, X_n$  be independent random variables in  $[a, b]$ , and  $\bar{X}_n = \frac{1}{n} \sum_{i=1}^n X_i$  their empirical mean. The empirical variance is defined as:*

$$V_n = \frac{1}{n-1} \sum_{i=1}^n (X_i - \bar{X}_n)^2.$$

For any  $\delta \in (0, 1)$  and  $n \geq 2$ , with probability at least  $1 - \delta$ :

$$\mathbb{E}[X] \leq \bar{X}_n + \sqrt{\frac{2V_n \ln(1/\delta)}{n}} + \frac{7(b-a) \ln(1/\delta)}{3(n-1)}.$$

## IV. Certified Radius Estimation in the Discrete Case

### A. Definitions and Notations

Let  $X = (X_1, \dots, X_m)$  follow a multinomial distribution with parameters  $n$  and  $p = (p_1, \dots, p_m)$ , where  $n$  is fixed and  $p_k = \mathbb{P}(f(x + \epsilon) = k)$ . The goal is to estimate a lower confidence bound for  $\theta := g(p)$ , assuming  $p \in \chi^{m-1} \subset \Delta^{m-1}$ .

The maximum likelihood estimator (MLE) of  $\theta$  is  $\hat{\theta} = g(\hat{p})$ , where  $\hat{p} = \frac{X}{n}$ . Define  $\Theta := g(\chi^{m-1})$  and  $\hat{\Theta} := g(\chi_n^{m-1})$ . For observed  $\tilde{\theta} \in \hat{\Theta}$ , denote the cumulative distribution function (CDF) of  $\hat{\theta}$  by  $\Pi(\cdot|p)$ :

$$\Pi(L) := 1 - \inf_{\substack{p \in \Delta^{m-1} \\ g(p) \leq L}} \Pi(\tilde{\theta}|p). \quad (3)$$

Simplifying for  $m \geq 3$ , reduce the multinomial parameter to  $q \in \Delta^2$  with  $q_1 = p_1$ ,  $q_2 = p_2$ , and  $q_3 = 1 - p_1 - p_2$ . If  $g$  depends only on  $p_1$  and  $p_2$ , then:

$$\Pi(\tilde{\theta}|p) = \Pi(\tilde{\theta}|q) = \sum_{\substack{x \in \Omega_n^2 \\ g(\frac{x}{n}) \leq \tilde{\theta}}} \binom{n}{x} q^x.$$

The lower confidence bound on  $\theta$  at level  $1 - \alpha$  is:

$$\hat{\theta} = \inf \{L \in \Theta : \Pi(L) = \alpha\}. \quad (4)$$

### B. First Radius Estimation

For the first radius,  $\chi^{m-1} = \Delta^{m-1}$ , so  $\Theta = [-1, 1]$  and  $\hat{\Theta} = \{-1, -1 + \frac{1}{n}, \dots, 1\}$ . Assuming the top two probabilities correspond to classes 1 and 2, the CDF simplifies to:

$$\Pi(\tilde{\theta} | p) = \mathbb{P}(X_1 - X_2 \leq k | q) \quad (5)$$

$$= \sum_{x_2=0}^n \sum_{x_1=0}^{\min(k+x_2, n)} \binom{n}{x} q^x. \quad (6)$$

---

### Algorithm 4: First Radius Estimation in the Discrete Case

---

**Input:** Counts  $X$ , threshold  $\epsilon > 0$ , routine `SolveSignomial(L)`

**Output:** Lower confidence bound  $\hat{\theta}$

```

1 Compute  $\tilde{\theta} \leftarrow \frac{X_1 - X_2}{n}$ 
2 Set bounds: left  $\leftarrow 0$ , right  $\leftarrow \tilde{\theta}$ 
3 while right - left >  $\epsilon$  do
4   |  $L \leftarrow \frac{\text{right} + \text{left}}{2}$ 
5   | Solution  $\leftarrow$  SolveSignomial(L)
6   | if Solution <  $1 - \alpha$  then
7   |   | right  $\leftarrow L$ 
8   | end
9   | else
10  |   | left  $\leftarrow L$ 
11  |   | end
12 end
13 return left

```

---

The lower confidence bound  $\hat{\theta}$  is computed by solving optimization problems in Eqs. (3) and (4). The high-level algorithm is:

For efficiency, approximate solutions can be used in early iterations, as justified by Lemma. A faster version of the algorithm is:

---

### Algorithm 5: Fast Radius Estimation in the Discrete Case

---

**Input:** Counts  $X$ , threshold  $\epsilon > 0$ , routines `SolveSignomial(L)` and `FastSolveSignomial(L)`

**Output:** Lower confidence bound  $\hat{\theta}$

```

1 Compute  $\tilde{\theta} \leftarrow \frac{X_1 - X_2}{n}$ 
2 Set bounds: left  $\leftarrow 0$ , right  $\leftarrow \tilde{\theta}$ , close  $\leftarrow$  False
3 while right - left >  $\epsilon$  do
4   |  $L \leftarrow \frac{\text{right} + \text{left}}{2}$ 
5   | if close then
6   |   | Solution  $\leftarrow$  SolveSignomial(L)
7   |   | end
8   |   | else
9   |   |   | Solution  $\leftarrow$  FastSolveSignomial(L)
10  |   |   | end
11  |   | if Solution <  $1 - \alpha$  then
12  |   |   | right  $\leftarrow L$ 
13  |   |   | end
14  |   | else
15  |   |   | close  $\leftarrow$  True
16  |   |   | left  $\leftarrow L$ 
17  |   |   | end
18  |   | end
19 return left

```

---

### C. Second Radius Estimation

We solve the following optimization problem:

$$\inf_{\substack{q \in \chi^2 \\ \Phi^{-1}(q_1) - \Phi^{-1}(q_2) \leq L}} \Pi(\tilde{\theta}|q). \quad (7)$$

Since  $\Phi^{-1}$  is not a posynomial or signomial function, the problem (7) cannot be solved directly. Using Taylor series approximation  $\Phi_M^{-1}$ , we reformulate the problem as:

$$\inf_{\substack{q \in \mathcal{X}^2 \\ \Phi_M^{-1}(q_1) - \Phi_M^{-1}(q_2) \leq L}} \Pi(\tilde{\theta}|q), \quad (8)$$

where  $\Pi(\tilde{\theta}|q)$  is redefined as:

$$\sum_{\substack{x \in \Omega_n^2 \\ \Phi_M^{-1}\left(\frac{x_1}{n}\right) - \Phi_M^{-1}\left(\frac{x_2}{n}\right) \leq \tilde{\theta}} \binom{n}{x} q^x. \quad (9)$$

Algorithm 6 summarizes the procedure:

---

**Algorithm 6:** Second Margin Estimation in the Discrete Case

---

**Input:** Counts  $X$ , threshold  $\epsilon > 0$ , routines `SolveSignomial(L)` and `FastSolveSignomial(L)`

- Output:** Lower confidence bound  $\underline{\theta}$  at confidence  $1 - \alpha$
- 1 Compute  $p_1$  using the Clopper-Pearson interval at level  $\frac{\alpha}{2}$ .  
   **if**  $p_1 > \frac{1}{2}$  **then**
  - 2   Compute  $\tilde{\theta} \leftarrow \Phi^{-1}\left(\frac{X_1}{n}\right) - \Phi^{-1}\left(\frac{X_2}{n}\right)$ . Solve the problem (??).
  - 3 **end**
  - 4 **else**
  - 5   Use the Bonferroni algorithm for standard confidence bounds.
  - 6 **end**
- 

## V. Certified Radius Estimation in the Continuous Case

### A. Estimating by Betting (Background)

[30] proposed confidence sequences (CS) for bounded random variables, allowing continuous monitoring with tighter bounds than empirical Bernstein’s inequality. The CS framework uses:

**Proposition 2** ([30]). *For i.i.d. random variables  $(X_t)_{t=1}^\infty$ , a  $(1 - \alpha)$ -CS for  $\mu$  is:*

$$C_t^{PrPI-EB} := \left( \frac{\sum_{i=1}^t \lambda_i X_i}{\sum_{i=1}^t \lambda_i} \pm \sqrt{\frac{2 \log(2/\alpha) + \sum_{i=1}^t v_i \psi_\epsilon(\lambda_i)}{\sum_{i=1}^t \lambda_i}} \right),$$

where  $\lambda_t^{PrPI-EB}$ ,  $\hat{\sigma}_t^2$ ,  $\hat{\mu}_t$ ,  $\psi_\epsilon(\lambda)$ , and  $v_i$  are defined in (??).

### B. First Radius Estimation

To certify the smoothed classifier, define  $Z := X^1 - \max_{j \neq 1} X^j$ , where each  $Z_i = X_i^1 - \max_{j \neq 1} X_i^j$ . The mean  $\bar{Z}$  is estimated conservatively using confidence intervals, applying Bonferroni correction or confidence sequences.

### C. Second Radius Estimation

For the second margin, define  $Z := \Phi^{-1}(X^1) - \max_{j \neq 1} \Phi^{-1}(X^j)$ . To handle unbounded  $\Phi^{-1}$ , we use Taylor

approximation  $\Phi_M^{-1}$ , ensuring boundedness. If  $\bar{X}^1 \geq \frac{1}{2}$ , the Taylor-based method is applied; otherwise, fallback to Bonferroni correction.

Lemma ensures approximation conservativeness. This process is detailed in Algorithm 6.

## VI. Experiments

### A. Certified Test-set Accuracy

Certified radius measures local classifier robustness but doesn’t capture the entire input space. The *certified test-set accuracy* (CTA) is a global measure for smoothed classifiers. Given a classifier  $g$ , test set  $S = \{(x_1, c_1), \dots, (x_N, c_N)\}$ , and radius  $r$ , we define:

$$z_i(r) = \mathbb{1}[g(x_i + \delta) = c_i \quad \forall \|\delta\|_2 < r]$$

The theoretical CTA is:

$$\text{CertAcc}_{\text{theo}}(r) = \frac{1}{N} \sum_{i=1}^N z_i(r)$$

For randomized smoothing classifiers, the theoretical CTA is approximated by:

$$\text{CertAcc}_{\text{approx}}(r) = \frac{1}{N} \sum_{i=1}^N Y_i(r)$$

where  $Y_i(r)$  denotes whether the certified radius of the smoothed classifier exceeds  $r$ . A one-sided confidence interval can be constructed for the unobserved  $\frac{1}{N} \sum_{i=1}^N z_i(r)$ .

### B. Results

We evaluate our radius estimation methods on the CIFAR-10 dataset. The base classifier is a 110-layer residual network [23] with Gaussian noise data augmentation. In all figures, CTA curves are based on margins instead of radii due to their direct proportionality.

Figure 3 compares certified accuracies on CIFAR-10 for various standard deviations. The CTA decreases as the standard deviation increases, as higher noise reduces the base accuracy, making classification harder.

Figure 4 and Table I show CTA results for different sample sizes and the impact of sample size and standard deviation on the CTA curve. The standard Bonferroni approach is conservative for small sample sizes, but as the sample size grows, the two curves converge. Differences are more pronounced at larger radii.

In the continuous case, in addition to the sample size and the standard deviation, another hyperparameter to consider is the *temperature*. The simplex map  $s$  used in the experiments is the tempered softmax function which is a generalization of the standard softmax function, introducing a temperature parameter to control the smoothness of the output distribution. Given a

TABLE I  
 CERTIFIED ACCURACY USING THE SECOND MARGIN ON THE CIFAR-10 DATASET IN THE DISCRETE CASE FOR DIFFERENT VALUES OF RADIUS  $r$  WITH A SAMPLE SIZE OF 100 AND A STANDARD DEVIATION  $\sigma = 0.12$ .

Method	Radius ( $r$ )									
	0.5	1.0	1.5	2.0	2.5	3.0	3.5	4.0	4.5	
CP + Bonferroni	0.774	0.744	0.720	0.662	0.582	0.000	0.000	0.000	0.000	0.000
Ours	0.780	0.746	0.726	0.670	0.614	0.538	0.538	0.538	0.538	0.538
Gain (%)	0.78%	0.27%	0.83%	1.21%	5.50%	$\infty$	$\infty$	$\infty$	$\infty$	$\infty$

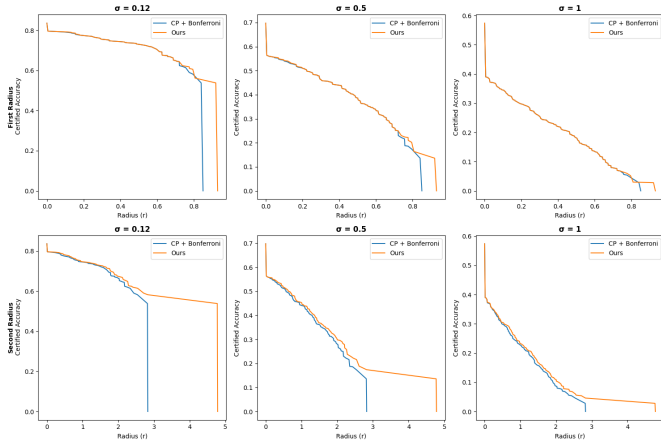


Fig. 3. Certified accuracies' comparison on the CIFAR-10 dataset in the discrete case for different standard deviations (displayed on the columns) with a sample size of 100. The legend and row conventions are the same as in Figure 4.

vector  $\mathbf{x} = (x_1, \dots, x_m)$  and a temperature parameter  $T > 0$ , the tempered softmax function  $\sigma_T : \mathbb{R}^m \rightarrow \mathbb{R}^m$  is defined as:

$$\sigma_T(\mathbf{x})_i = \frac{\exp(x_i/T)}{\sum_{j=1}^m \exp(x_j/T)}$$

for  $i = 1, \dots, m$ .

As  $T \rightarrow 0^+$ , the tempered softmax approaches a hard maximum (one-hot vector). As  $T \rightarrow \infty$ , the tempered softmax approaches a uniform distribution. When  $T = 1$ , it reduces to the standard softmax function.

Figures 5 & 6 and tables II & III show the effect of increasing the number of samples  $n$  and increasing the standard deviation  $\sigma$  respectively. The effects of these hyperparameters are similar in both discrete and continuous case.

It is clear from Figure 7 that increasing the temperature parameter  $T$  reduces the discrepancies between the Bonferroni approach and our new method. Higher temperatures lead to softer decision boundaries. As the temperature increases, the output probabilities of the tempered softmax function become more uniform, regardless of the input values. This means that the function becomes less sensitive to differences in the input, causing different methods to produce more similar outputs. Hence, as the temperature rises, the tempered softmax function becomes less responsive to changes in its inputs. This means that larger changes in the input are required to produce the same

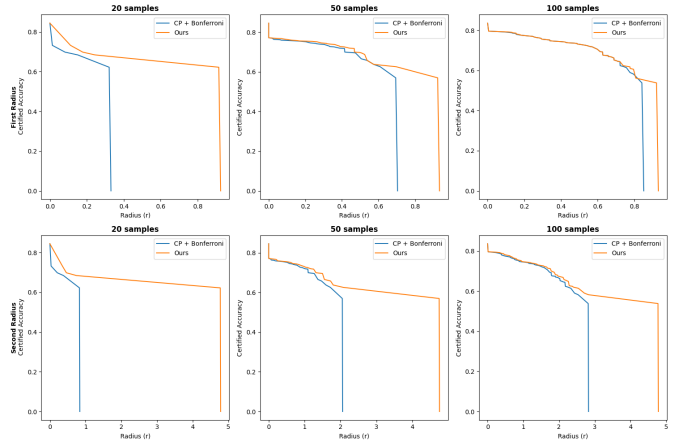


Fig. 4. Certified accuracies' comparison on the CIFAR-10 dataset in the discrete case for different numbers of samples (displayed on the columns) with  $\sigma = 0.12$ . CP + Bonferroni means Clopper-Pearson interval with Bonferroni correction, and Ours means our new approach in section IV. The first row compares the certified accuracies using the first margin and the second row compares the certified accuracies using the second margin.

change in output probabilities. Consequently, the differences between various methods become less pronounced. At lower temperatures, the tempered softmax accentuates differences between inputs. The highest value tends to dominate, resulting in an output distribution that's closer to a one-hot vector.

## VII. Conclusion and Future Work

In this paper, we have presented novel techniques for improving the estimation of certified radii in randomized smoothing, leading to tighter bounds on certified test-set accuracy. Our methods have demonstrated significant improvements on both CIFAR-10 and ImageNet datasets, showcasing the potential for more efficient and accurate certification of neural network robustness against adversarial perturbations. While our results mark a substantial step forward in the field of adversarial robustness, they also open up several promising avenues for future research: One particularly intriguing direction is the development of more efficient tricks for estimating certified radii in discrete domains. In the continuous case, our work has highlighted the importance of tight confidence intervals for accurate estimation of certified radii, leaving the exploration of tighter confidence sequences and the development of new

TABLE II

CERTIFIED ACCURACY USING THE FIRST MARGIN ON CIFAR-10 IN THE CONTINUOUS CASE FOR DIFFERENT VALUES OF RADIUS  $r$  AND SAMPLE SIZES WITH  $\sigma = 0.5$  AND A TEMPERATURE OF 1.

Samples	Method	Radius ( $r$ )								
		0.1	0.2	0.3	0.4	0.5	0.6	0.7	0.8	0.9
100	CS + Bonferroni	0.400	0.347	0.289	0.220	0.157	0.066	0.000	0.000	0.000
	CS + Ours	0.419	0.362	0.303	0.239	0.173	0.092	0.000	0.000	0.000
	Comparison (%)	4.69%	4.28%	5.04%	8.70%	10.65%	39.16%	N/A	N/A	N/A
300	CS + Bonferroni	0.526	0.464	0.411	0.354	0.296	0.233	0.173	0.101	0.000
	CS + Ours	0.536	0.471	0.416	0.361	0.301	0.239	0.179	0.105	0.000
	Comparison (%)	1.93%	1.55%	1.39%	1.89%	1.94%	2.52%	3.49%	4.06%	N/A
500	CS + Bonferroni	0.560	0.490	0.434	0.379	0.322	0.261	0.199	0.133	0.050
	CS + Ours	0.568	0.497	0.442	0.383	0.329	0.266	0.202	0.136	0.054
	Comparison (%)	1.43%	1.33%	2.00%	0.99%	2.08%	2.01%	1.89%	2.33%	9.21%

TABLE III

CERTIFIED ACCURACY USING THE SECOND MARGIN ON CIFAR-10 IN THE CONTINUOUS CASE FOR DIFFERENT VALUES OF RADIUS  $r$  AND SAMPLE SIZES WITH  $\sigma = 0.5$  AND A TEMPERATURE OF 1.

Samples	Method	Radius ( $r$ )								
		0.1	0.2	0.3	0.4	0.5	0.6	0.7	0.8	0.9
100	CS + Bonferroni	0.436	0.415	0.393	0.369	0.352	0.328	0.305	0.284	0.259
	CS + Ours	0.437	0.418	0.401	0.383	0.373	0.364	0.359	0.354	0.347
	Comparison (%)	0.19%	0.83%	1.91%	3.72%	5.95%	11.17%	17.68%	24.67%	34.03%
300	CS + Bonferroni	0.572	0.545	0.518	0.493	0.471	0.451	0.431	0.413	0.391
	CS + Ours	0.572	0.547	0.523	0.500	0.481	0.465	0.451	0.439	0.427
	Comparison (%)	0.00%	0.42%	0.92%	1.46%	2.15%	2.97%	4.59%	6.25%	9.24%
500	CS + Bonferroni	0.600	0.578	0.553	0.525	0.500	0.478	0.457	0.437	0.419
	CS + Ours	0.600	0.578	0.556	0.530	0.509	0.489	0.473	0.461	0.448
	Comparison (%)	0.08%	0.08%	0.53%	1.03%	1.77%	2.29%	3.50%	5.62%	6.98%

theoretical frameworks that provide rigorous backing for the tightness of these improved confidence intervals for future work. By pursuing these lines of research, we hope to further narrow the gap between empirical performance and theoretical guarantees in randomized smoothing. We leave for future the comparison between empirical certified radii (like those based on PGD attacks) and estimated certified radii.

## Appendix

### A. Definitions

In signomial programming, the building block is a **monomial** function which is a function of the form

$$f(\mathbf{x}) = cx_1^{a_1} x_2^{a_2} \dots x_m^{a_m}$$

where:

- $c > 0$  is a positive coefficient,
- $\mathbf{x} = (x_1, x_2, \dots, x_m)$  are positive variables,

- $a_1, a_2, \dots, a_m$  are real exponents (not necessarily non-negative).

Building on top of this definition, we can define two types of functions. A **posynomial** function is a sum of monomials, while a **signomial** function is a linear combination of monomials (meaning that the multiplicative coefficients can be negative).

A signomial program (SP) is an optimization problem of the form:

$$\begin{aligned} & \text{minimize} && f_0(\mathbf{x}) \\ & \text{subject to} && f_i(\mathbf{x}) \geq 0, \quad i = 1, \dots, p \\ & && \mathbf{x} > 0 \end{aligned}$$

where:

- $\mathbf{x} = (x_1, \dots, x_m)$  is the vector of optimization variables,
- $f_0, f_1, \dots, f_m$  are signomial functions.

Signomials programs generalize the well-known geometric programs that are much easier to solve, since they can be reduced to convex optimization problems. However, signomial programs are generally non-convex optimization problems and

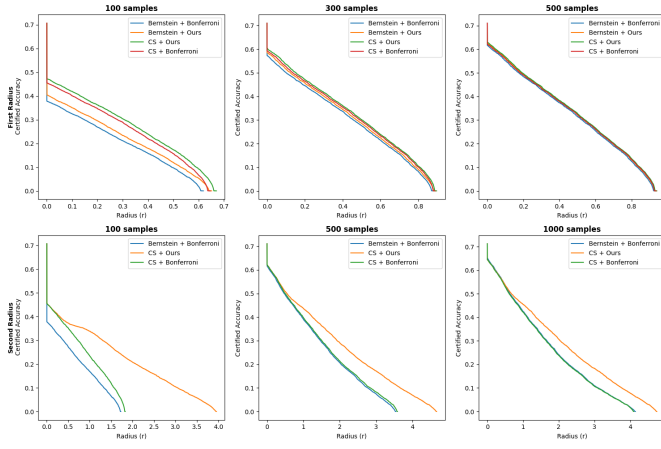


Fig. 5. Certified accuracies' comparison on the CIFAR-10 dataset in the continuous case for different sample sizes (displayed on the columns) with  $\sigma = 0.5$  and a temperature equal to 1. CS/Bernstein + Bonferroni stands for the Bonferroni approach with either the empirical Bernstein interval (Proposition 1) or the confidence sequence (Proposition 2), and CS/Bernstein + Ours stands for the new approach in section V, where the interval used is either the empirical Bernstein interval or the confidence sequence as before. The first row compares the certified accuracies using the first margin and the second row compares the certified accuracies using the second margin.

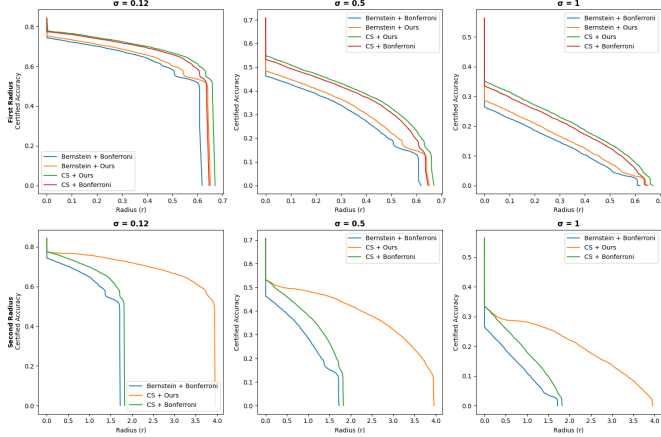


Fig. 6. Certified accuracies' comparison on the CIFAR-10 dataset in the continuous case for different standard deviations (displayed on the columns) with a sample size of 100 and a temperature equal to 0.1. The legend and row conventions are the same as in Figure 5.

can be challenging to solve globally. Various techniques, such as successive convex approximation or branch-and-bound methods, are often employed to find solutions to SPs.

## B. Proof of Lemma

*Proof.* Suppose there exists  $q^0 \in \Delta^2$  such that  $q_1^0 - q_2^0 \leq L$  and  $\Pi(\tilde{\theta}|q^0) \leq 1 - \alpha$  for some  $L \in \Theta$ . It follows that

$$\inf_{\substack{q \in \Delta^2 \\ q_1 - q_2 \leq L}} \Pi(\tilde{\theta}|q) \leq \Pi(\tilde{\theta}|q^0) \leq 1 - \alpha.$$

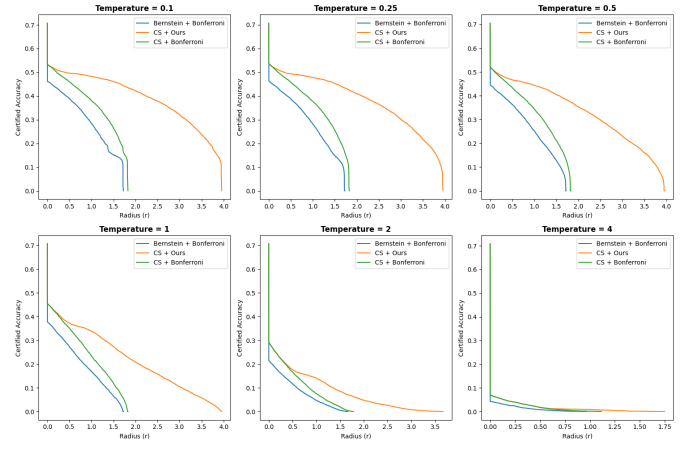


Fig. 7. Certified accuracies' comparison on the CIFAR-10 dataset in the continuous case for different temperatures (displayed on the columns) with a sample size of 100 and  $\sigma = 0.5$ . The legend and row conventions are the same as in Figure 5.

In other terms,

$$\alpha \leq \Pi(L).$$

Since  $\Pi$  is nondecreasing, by definition of  $\hat{\theta}$ ,

$$\Pi(\hat{\theta}) \leq \alpha.$$

Therefore,  $\Pi(\hat{\theta}) \leq \Pi(L)$ , which implies  $\hat{\theta} \leq L$ .  $\square$

## C. Proof of Lemma

*Proof.* To recall, the error function, denoted as  $\text{erf}(x)$ , is defined as

$$\text{erf}(x) = \frac{2}{\sqrt{\pi}} \int_0^x e^{-t^2} dt.$$

Its domain of the error function is the interval  $(-\infty, \infty)$ , and its codomain is the interval  $(-1, 1)$ . The error function is an increasing and odd function.

The inverse error function, denoted as  $\text{erf}^{-1}(z)$ , is the inverse of the error function. Its domain is the interval  $(-1, 1)$ , and its codomain is all real numbers. Due to the complexity of the error function, the inverse error function does not have a simple closed-form expression. However, it can be approximated using various methods.

One such approximation for the inverse error function is given by the following series:

$$\text{erf}^{-1}(x) = \sum_{k=0}^{\infty} \frac{c_k}{2k+1} \left( \frac{\sqrt{\pi}}{2} x \right)^{2k+1}$$

where  $c_0 = 1$  and the subsequent coefficients  $c_k$  are defined recursively as:

$$c_k = \sum_{m=0}^{k-1} \frac{c_m c_{k-1-m}}{(m+1)(2m+1)}.$$



This series approximation converges on the entire domain of the inverse error function. If we denote by  $\text{erf}_M$  the  $M$ -th order Taylor series of the error function,

$$\text{erf}_M(x) := \sum_{k=0}^M \frac{c_k}{2k+1} \left( \frac{\sqrt{\pi}}{2} x \right)^{2k+1},$$

then it is clear that  $\text{erf}(x) \geq \text{erf}_M(x)$  if  $x \geq 0$ , and  $\text{erf}(x) \leq \text{erf}_M(x)$  otherwise.

The Gaussian quantile function, denoted as  $\Phi^{-1}$ , can be expressed in terms of the inverse error function as follows

$$\Phi^{-1}(p) = \sqrt{2} \cdot \text{erf}^{-1}(2p - 1).$$

The domain of  $\Phi^{-1}(p)$  is  $(0, 1)$ , corresponding to probabilities, while its codomain is  $\mathbb{R}$ . The Taylor series approximation of  $\text{erf}^{-1}(x)$  naturally leads to an approximation of the Gaussian quantile function. By substituting  $x = 2p - 1$  into the Taylor series for  $\text{erf}^{-1}(x)$  and multiplying by  $\sqrt{2}$ , we obtain

$$\Phi^{-1}(p) \approx \sqrt{2} \sum_{k=0}^M \frac{c_k}{2k+1} \left( \frac{\sqrt{\pi}}{2} (2p - 1) \right)^{2k+1} := \Phi_M^{-1}(p)$$

It follows that if  $p \geq \frac{1}{2}$ , then  $\Phi^{-1}(p) \geq \Phi_M^{-1}(p)$ , and if  $p \leq \frac{1}{2}$ , then  $\Phi^{-1}(p) \leq \Phi_M^{-1}(p)$ , which concludes the proof.  $\square$

We conducted our experiments on the ImageNet dataset in the same way as in Section VI. The only difference is that we used a 50-layer residual network instead of the 110-layer one. The figures of the Imagenet dataset (8, 9, 10, and 11) are consistent with our previous findings on the CIFAR-10 dataset.

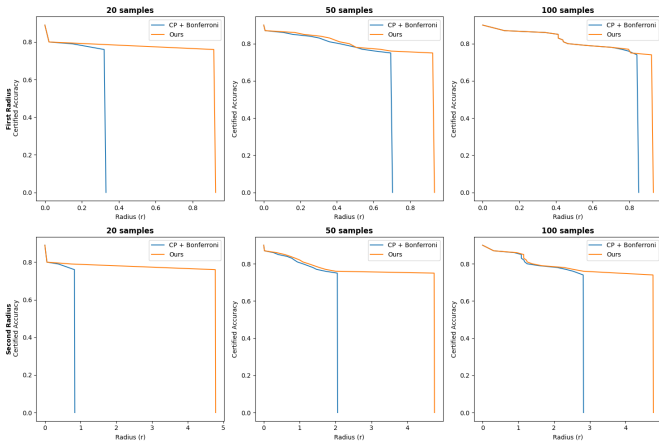


Fig. 8. Certified accuracies' comparison on the ImageNet dataset in the discrete case for different numbers of samples (displayed on the columns) with  $\sigma = 0.25$ .

## References

- [1] A. Krizhevsky, I. Sutskever, and G. E. Hinton, "Imagenet classification with deep convolutional neural networks," in *Advances in neural information processing systems*, 2012, pp. 1097–1105.
- [2] J. Devlin, M.-W. Chang, K. Lee, and K. Toutanova, "Bert: Pre-training of deep bidirectional transformers for language understanding," *arXiv preprint arXiv:1810.04805*, 2018.

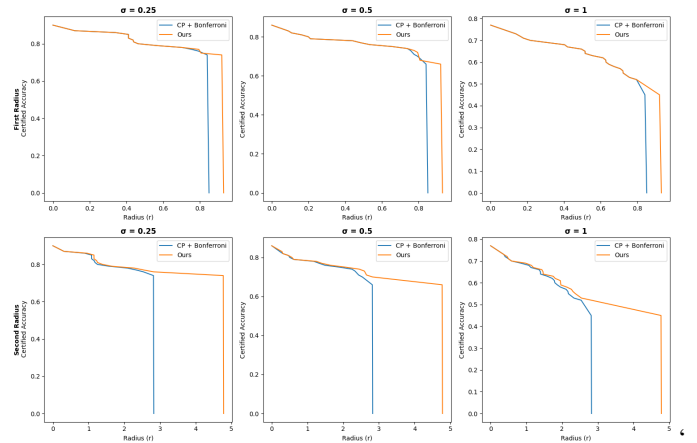


Fig. 9. Certified accuracies' comparison on the ImageNet dataset in the discrete case for different standard deviations (displayed on the columns) with a sample size of 100.

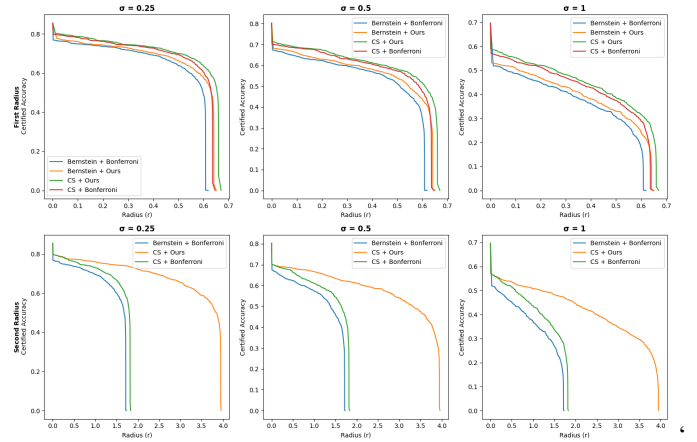


Fig. 10. Certified accuracies' comparison on the ImageNet dataset in the continuous case for different standard deviations (displayed on the columns) with a sample size of 100 and a temperature equal to 0.5.

- [3] Y. LeCun, Y. Bengio, and G. Hinton, "Deep learning," *Nature*, vol. 521, no. 7553, pp. 436–444, 2015.
- [4] I. Goodfellow, Y. Bengio, and A. Courville, *Deep learning*. MIT press, 2016.
- [5] B. Biggio and F. Roli, "Wild patterns: Ten years after the rise of adversarial machine learning," *Pattern Recognition*, vol. 84, pp. 317–331, 2018.
- [6] Y. Vorobeychik and M. Kantarcioglu, *Adversarial machine learning*. Morgan & Claypool, 2018.
- [7] C. Szegedy, W. Zaremba, I. Sutskever, J. Bruna, D. Erhan, I. Goodfellow, and R. Fergus, "Intriguing properties of neural networks," *arXiv preprint arXiv:1312.6199*, 2013.
- [8] I. J. Goodfellow, J. Shlens, and C. Szegedy, "Explaining and harnessing adversarial examples," *arXiv preprint arXiv:1412.6572*, 2014.
- [9] N. Carlini and D. Wagner, "Towards evaluating the robustness of neural networks," in *2017 IEEE Symposium on Security and Privacy (SP)*. IEEE, 2017, pp. 39–57.

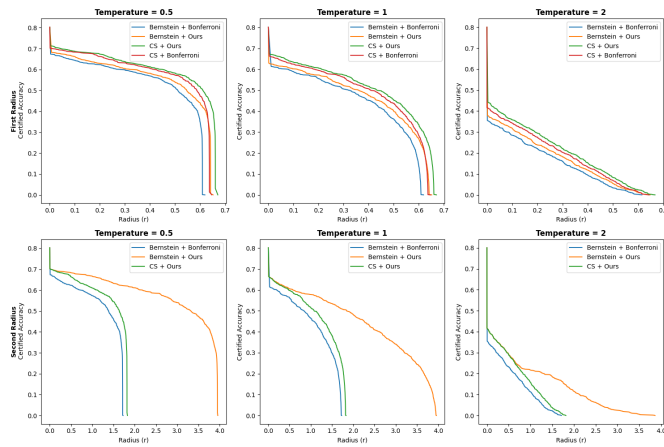


Fig. 11. Certified accuracies' comparison on the CIFAR-10 dataset in the continuous case for different temperatures (displayed on the columns) with a sample size of 100 and  $\sigma = 0.5$ .

- [10] —, “Audio adversarial examples: Targeted attacks on speech-to-text,” in *2018 IEEE Security and Privacy Workshops (SPW)*. IEEE, 2018, pp. 1–7.
- [11] A. Kurakin, I. Goodfellow, and S. Bengio, “Adversarial examples in the physical world,” *arXiv preprint arXiv:1607.02533*, 2016.
- [12] K. Eykholt, I. Evtimov, E. Fernandes, B. Li, A. Rahmati, C. Xiao, A. Prakash, T. Kohno, and D. Song, “Robust physical-world attacks on deep learning visual classification,” in *Proceedings of the IEEE Conference on Computer Vision and Pattern Recognition*, 2018, pp. 1625–1634.
- [13] S. G. Finlayson, H. W. Chung, I. S. Kohane, and A. L. Beam, “Adversarial attacks against medical deep learning systems,” *arXiv preprint arXiv:1804.05296*, 2019.
- [14] S. Gu and B. T. Kelly, “Adversarial deep learning for robust detection of binary trading signals,” *arXiv preprint arXiv:1810.08295*, 2018.
- [15] B. Li, Y. Wang, and L. Zhang, “Adversarial attacks on financial deep learning models,” *arXiv preprint arXiv:2004.05150*, 2020.
- [16] F. Tramèr, A. Kurakin, N. Papernot, I. Goodfellow, D. Boneh, and P. McDaniel, “Ensemble adversarial training: Attacks and defenses,” *arXiv preprint arXiv:1705.07204*, 2017.
- [17] C. Guo, M. Rana, M. Cisse, and L. Van Der Maaten, “Countering adversarial images using input transformations,” *arXiv preprint arXiv:1711.00117*, 2017.
- [18] J. H. Metzen, T. Genewein, V. Fischer, and B. Bischoff, “On detecting adversarial perturbations,” *arXiv preprint arXiv:1702.04267*, 2017.
- [19] D. Tsipras, S. Santurkar, L. Engstrom, A. Turner, and A. Madry, “Robustness may be at odds with accuracy,” *arXiv preprint arXiv:1805.12152*, 2018.
- [20] W. Xu, D. Evans, and Y. Qi, “Feature squeezing: Detecting adversarial examples in deep neural networks,” in *Network and Distributed System Security Symposium*, 2017.
- [21] V. Tjeng, K. Xiao, and R. Tedrake, “Evaluating robustness of neural networks with mixed integer programming,” in *International Conference on Learning Representations*, 2017.
- [22] G. Katz, C. Barrett, D. L. Dill, K. Julian, and M. J. Kochenderfer, “Reluplex: An efficient smt solver for verifying deep neural networks,” in *International Conference on Computer Aided Verification*. Springer, 2017, pp. 97–117.
- [23] J. Cohen, E. Rosenfeld, and Z. Kolter, “Certified adversarial robustness via randomized smoothing,” in *International Conference on Machine Learning*. PMLR, 2019, pp. 1310–1320.
- [24] A. Raghunathan, J. Steinhardt, and P. Liang, “Semidefinite relaxations for certifying robustness to adversarial examples,” in *Advances in Neural Information Processing Systems*, 2018, pp. 10900–10910.
- [25] E. Wong and J. Z. Kolter, “Provable defenses against adversarial examples via the convex outer adversarial polytope,” in *International Conference on Machine Learning*. PMLR, 2018, pp. 5286–5295.
- [26] B. Delattre, A. Araujo, Q. Barthélemy, and A. Allauzen, “The lipschitz-variance-margin tradeoff for enhanced randomized smoothing,” 2024. [Online]. Available: <https://arxiv.org/abs/2309.16883>
- [27] J. Bridle, “Training stochastic model recognition algorithms as networks can lead to maximum mutual information estimation of parameters,” in *Advances in Neural Information Processing Systems*, D. Touretzky, Ed., vol. 2. Morgan-Kaufmann, 1989. [Online]. Available: [https://proceedings.neurips.cc/paper\\_files/paper/1989/file/0336dcbab05b9d5ad24f4333c7658a0e-Paper.pdf](https://proceedings.neurips.cc/paper_files/paper/1989/file/0336dcbab05b9d5ad24f4333c7658a0e-Paper.pdf)
- [28] A. Martins and R. Astudillo, “From softmax to sparsemax: A sparse model of attention and multi-label classification,” in *Proceedings of The 33rd International Conference on Machine Learning*, ser. Proceedings of Machine Learning Research, M. F. Balcan and K. Q. Weinberger, Eds., vol. 48. New York, New York, USA: PMLR, 20–22 Jun 2016, pp. 1614–1623. [Online]. Available: <https://proceedings.mlr.press/v48/martins16.html>
- [29] A. Maurer and M. Pontil, “Empirical Bernstein bounds and sample variance penalization,” 2009. [Online]. Available: <https://arxiv.org/abs/0907.3740>
- [30] I. Waudby-Smith and A. Ramdas, “Estimating means of bounded random variables by betting,” 2022. [Online]. Available: <https://arxiv.org/abs/2010.09686>